Combined Co- and Cross-Polarized SAR Measurements Under Extreme Wind Conditions

Alexis A. Mouche, Bertrand Chapron, Biao Zhang, *Senior Member, IEEE*, and Romain Husson

Abstract— **During summer 2016, the European Space Agency (ESA) set up the Satellite Hurricane Observations Campaign, a campaign dedicated to hurricane observations with Sentinel-1 synthetic aperture radar (SAR) in both vertical-vertical (VV) and vertical-horizontal (VH) polarizations acquired in wide swath modes. Among the 70 Sentinel-1 passes scheduled by the ESA mission planning team, more than 20 observations over hurricane eyes were acquired and tropical cyclones were captured at different development stages. This enables us to detail the sensitivity difference of VH and VV normalized radar cross section (NRCS) to the response of intense ocean surface winds. As found, the sensitivity of the VH-NRCS computed at 3-km resolution is reported to be more than 3.5 times larger than in VV. Taking opportunity of SAR high resolution, we also show that the decrease in resolution (up to 25 km) does not dramatically change the sensitivity difference between VV and VH polarizations. For wind speeds larger than 25 m/s, a new geophysical model function (MS1A) to interpret cross-polarized signal is proposed. Both channels are then combined to get ocean surface wind vectors. SAR winds are further compared at 40-km resolution against L-band soil moisture active and passive mission (SMAP) radiometer winds with co-locations less than 30 min. Overall excellent consistency is found between SMAP and this new SAR winds. This paper opens perspectives for MetOp-SG SCA, the next-generation C-band scatterometer with co- and cross-polarization capability.**

Index Terms— **Cross-polarization and co-polarization radar cross section, high-resolution extreme ocean surface winds, hurricanes, microwave, scattering, space-borne radar, typhoon.**

I. Introduction

TODAY, the ever-increasing sampling capability of satellite active and passive microwave observations, including high-resolution imaging radar instruments, certainly opens for new opportunities to derive improved surface wind forcing properties. While both physics of the ocean surface and of the remote sensing measurements are still imperfectly understood, numerous satellite radar measurements at C-band have now routinely demonstrated the potential to provide unique ocean surface imprints of extreme atmospheric phenomena (see [1], [2]). Among available satellite observations, synthetic aperture radar (SAR) measurements are quite unique in providing the necessary swath coverage and very high resolution capability to help characterize the inner core storm structures, such as, the eyewalls and radius of maximum wind (RMW) speed, and/or the rain band locations. For tropical cyclones (TCs), backscatter signals systematically display strong variations, likely corresponding to strong gradients in ocean surface wind speeds and directions, and/or related to the signatures of heavy rain precipitations.

Moreover, available C-band SAR cross-polarized [CP for vertical-horizontal (VH) or horizonal-vertical (HV)] measurements generally exhibit largely improved sensitivity compared with conventional co-polarized [vertical-vertical (VV) or horizontal-horizontal (HH)] acquisitions (see [2], [3]). Over rain-free areas, the remote sensing sensitivity at very high wind speed is anticipated to be mostly controlled by the sensor capability to directly or indirectly probe the wave breaking impacts. Already under moderate wind speeds, CP backscatter variations were shown to efficiently trace local breaking and near-breaking areas, caused by ocean surface current variations [4]. For TC conditions, this CP sensitivity to breaking events can further likely explain the unambiguously reported capabilities to retrieve strong wind gradient information (see [5], [6]). At very high winds, the C-band CP signals are further weakly dependent upon incidence angles, and more importantly, almost insensitive to wind direction. Such a property can thus help constrain the use of the co-polarized (VV or HH) measurements, to retrieve the surface wind vector information from single-antenna SAR instruments [7].

Hereafter, a standard procedure to retrieve surface wind information from single-antenna SAR observations (see [8], [9]) is then extended to consistently consider and combine CP measurements. After Radarsat-2, high-resolution C-band ocean backscatter CP signals are now routinely collected by the European satellite missions, Sentinel-1 A (S-1A) and B (S-1B), respectively, launched in 2014 and 2016. Measurements are of sufficiently high accuracy [10], to test and extend this methodology, opening perspectives for hurricane studies with enhanced revisit times. The high-resolution

Manuscript received April 3, 2017; revised June 5, 2017; accepted July 15, 2017. This work was supported in part by the National Science Foundation of China for Outstanding Young Scientist under Grant 41622604, in part by the Excellent Youth Science Foundation of Jiangsu Province under Grant BK20160090, in part by the ESA SEOM (S1OceanStudy) program, in part by ESA Dragon-4 Program, and in part by ESA SMOS-STORM CCN contract. *(Corresponding author: Alexis A. Mouche.)*

A. A. Mouche is with the Laboratoire d'Océanographie Physique Spatiale, 29280 Plouzane, France, and also with the Nanjing University of Information Science and Technology, Nanjing 210044, China (e-mail: alexis.mouche@ifremer.fr).

B. Chapron is with the Laboratoire d'Océanographie Physique Spatiale, 29280 Plouzane, France.

B. Zhang is with the Nanjing University of Information Science and Technology, Nanjing 210044, China.

R. Husson is with Collecte Localisation Satellites, 29280 Plouzane, France.

Color versions of one or more of the figures in this paper are available online at http://ieeexplore.ieee.org.

Digital Object Identifier 10.1109/TGRS.2017.2732508

SAR observations can further be used to more precisely investigate resolution issues, certainly affecting lower resolved active (e.g., ASCAT scatterometer) or passive (radiometer) observations.

In this paper, we focus on a dedicated Sentinel-1 hurricane acquisition campaign that acquired more than 20 hurricane eye hits. This relatively large data set can help to more precisely assess the Sentinel-1 measurement capabilities and their differing sensitivity under extreme conditions, as well as to test and apply the proposed approach combining co- and cross-polarized signals to estimate high-resolution wind vector fields. Of particular interest for this analysis, the L-band passive microwave measurements from soil moisture active and passive mission (SMAP) can be precisely colocated with Sentinel-1A acquisitions, with time differences of less than 15 min. For rapidly evolving phenomena, such as TC, this small time difference between the two sensors is crucial to ensure almost contemporaneous comparisons. As understood, upwelling radiation measurements at L-band (1.4 GHz) are significantly less affected by rain and atmospheric effects than at higher microwave frequencies (see [11]), and offer new opportunities to complement existing ocean satellite TC observations (see [12], [13]). Analysis and comparisons are thus performed to directly relate the active C-band co- and cross-polarized high-resolution backscattered signals and the medium-resolution passive L-band brightness temperatures. The data used for this paper are presented in Section II. Section III deals with their analysis and a new wind inversion method combining both co-polarization and cross polarization is introduced. Section IV concludes this paper and summarizes the principal results.

II. Data Sets

Accumulating a collection of hurricane SAR observations represents a major challenge. Contrary to most other polar-orbit missions, SAR missions do not continuously acquire data, and follow a predefined mission planning. Starting in 1999, the hurricane watch program tried to mitigate this expected data serendipity. This program evolved from archival data searches to storm monitoring, with dedicated planning, to enable coincident acquisitions with National Oceanic and Atmospheric Administration (NOAA) aircraft penetration flights according to the forecast of hurricane trajectory [14]. Today, such a program solely applies to Radarsat-2 data within the framework of the Canadian hurricane watch program. While Sentinel-1A and B are jointly operating to offer an improved coverage, there is no Sentinel-based Copernicus service dedicated to extreme winds monitoring. For the 2014 and 2015 TC seasons, only four Sentinel-1 acquisitions were obtained, and only one with cross-polarized signal. To further note, NOAA aircraft surveys are available only in the West Atlantic and East Pacific regions.

A. Sentinel-1 SAR Data During the Satellite Hurricane Observation Campaign

To maximize SAR acquisitions during the 2016 hurricane season, a dedicated campaign, Satellite Hurricane Observation Campaign (SHOC), was designed with the European Space Agency (ESA) Sentinel-1 mission planning team to trigger late programming acquisitions based on hurricane tracks forecasts. Tracks were provided by NOAA over the Atlantic, Central, and Eastern Pacific regions and by National Meteorological Center of the China Meteorological Administration over the Western Pacific Ocean. SAR acquisitions were performed in VV+VH polarizations. The extended wide swath (EW) mode was the highest priority, as its noise equivalent sigma zero (NESZ) is expected to be lower than for the interferometric wide swath mode [10]. An EW swath is 400-km wide and covers incidence angles from about 17° to 45°. The NESZ is different for each subswath, and further range dependent inside each subswath (see [10, Fig. 2]).

TABLE I

List of Hurricanes' Names Whose Eye Was Captured by Sentinel-1A With Corresponding Acquisition Date, Start UTC Time, Stop UTC Time, and Acquisition Mode

Hurricane Name	Date	UTC Start	UTC Stop	Acq. Mode	Polarization
Gaston	2016-08-26	21:15:05	21:18:09	EW	VV+VH
Gaston	2016-08-27	09:21:24	09:24:14	EW	VV+VH
Gaston	2016-08-29	21:40:21	21:43:42	EW	VV+VH
Gaston	2016-08-30	09:44:12	09:47:44	EW	VV+VH
Gaston	2016-09-01	20:29:25	20:31:08	EW	VV+VH
Gaston	2016-09-02	08:28:58	08:31:20	EW	VV+VH
Hermine	2016-09-01	23:43:24	23:45:59	IW	VV+VH
Hermine	2016-09-04	22:31:53	22:35:04	EW	VV+VH
Karl	2016-09-20	09:23:23	09:26:52	EW	VV+VH
Karl	2016-09-23	22:20:28	22:24:31	EW	VV+VH
Lester	2016-08-26	13:39:53	13:40:56	EW	VV+VH
Lester	2016-08-30	14:45:12	14:46:58	EW	VV+VH
Lester	2016-08-31	03:15:20	03:17:12	EW	VV+VH
LyonRock	2016-08-27	20:49:54	20:54:54	EW	VV+VH
LyonRock	2016-08-29	20:34:10	20:37:49	EW	VV+VH
Megi	2016-09-26	09:33:48	09:37:14	EW	VV+VH
Namtheum	2016-09-04	09:19:28	09:24:32	EW	VV+VH

Among the 70 Sentinel-1 passes scheduled by the ESA mission planning team, more than 20 hurricane eye hits were gathered, and TCs could be intercepted at very different development stages. TCs such as Lester and Gaston were imaged by Sentinel-1 up to ten times, including acquisitions during intensification stages. Fig. 1(a) illustrates the set of six Sentinel-1A acquisitions in EW mode over the hurricane Lester in the Pacific Ocean. The most intense winds were captured over the super typhoon Lyonrock and the hurricane Lester, both reaching Category-4 on the Saffir–Simpson wind scale at acquisition time, with maximum sustained winds (MSWs) up to 115 and 120 knots, respectively, as predicted by the track analysis. The list of the cases considered in this paper is reported in Table I.

After the NESZ is estimated over low wind areas, all products were corrected from noise (see [10]). Normalized radar cross sections (NRCSs) were computed at a spatial resolution of 1 km, and further averaged at 3, 25, 40, and 50 km. Fig. 1(b) and (c) shows an example of Sentinel-1 acquisition in EW over Lester on August 31, 2016, between 03:15:20 and 03:17:12 UTC in both VV and VH polarizations.

B. External Data

Based on the analysis of cloud patterns in visible and infrared imagery from geostationary and polar-orbiting satellites, the Dvorak technique allows operational experts to provide information on the storms intensity evolution and the structural state of the wind system [15]. Over its area of

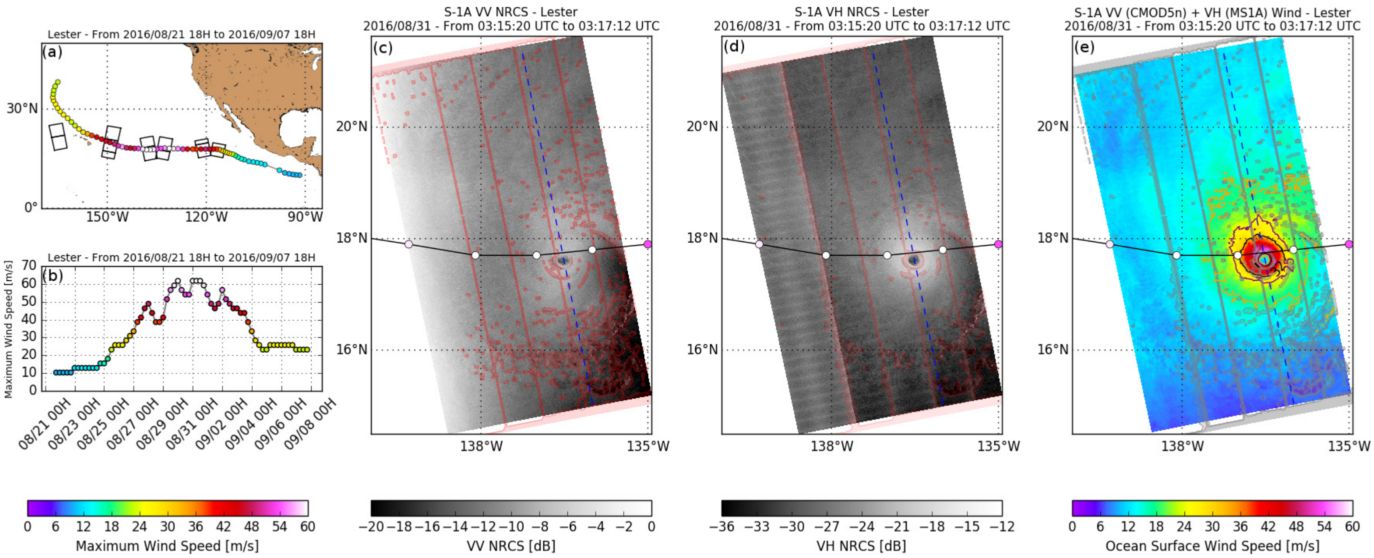

Fig. 1. Example of SAR EW acquisitions for Lester hurricane from August 20, 2016 to September 8, 2016. (a) Hurricane track map with corresponding maximum surface wind speed in color. (b) History of maximum surface wind speed. (c) VV-NRCS map acquired in EW mode on August 31, 2016 at 03:16 UTC. (d) Same for VH-NRCS. (e) Ocean surface wind speed obtained with the method presented in this paper.

responsibility, the Joint Typhoon Warning Center applies this technique as primary means to estimate intensity. Every 6 h, the TC is characterized through several parameters, such as the MSW, defined as the 1-min average wind speed at 10-m height above the surface, the RMW, and the maximum radial extent of significant wind speed thresholds (i.e., the radial extent of 34-, 50-, and 64-knot wind speed) in each geographical quadrant [16]. Once the hurricane season completed, operational estimates of these parameters are revised, and available as best tracks estimates.

Thanks to the phasing of its near-polar orbit and its very large swath, SMAP L-band brightness temperature data can be co-located with Sentinel-1A acquisitions, with time differences of less than 30 min. Our analysis of co-location opportunities with other sensors such as AMSR-2, ASCAT-A, ASCAT-B, or windsat reveals much less favorable time differences with Sentinel-1A acquisitions. Somehow commensurate to C-band CP measurements, L-band brightness temperature measurements have been found to monotonically increase with TC intensity. In line with the SMOS data analysis by [12], [13] and [17] proposed to interpret the sensitivity of SMAP measurements in terms of surface wind. Over the wind speed range of 0–20 m/s, [13] found a bias of the SMAP radiometer wind speed products computed with respect to the WindSat or SSMIS wind speed under 0.5 m/s and root-mean-square difference (RMSD) about 1.7 m/s. The analysis of eight TCs by [17] against SFMR revealed bias of 0.64 m/s and standard deviation of 3.11 m/s. Comparison from [13] with the SFMR winds indicates an RMSD of about 4.6 m/s for wind speeds in the range of 20–40 m/s. For the wind direction, [13] reported an RMSD between SMAP radiometer wind and ECMWF analysis of 18.4° for wind speeds in the range of 12–30 m/s. They also underline that the wind direction retrieved from SMAP radiometer data above 30 m/s remains unvalidated due to a lack of accurate wind direction for error assessment. In addition, [17] notes that SMAP has a limited capability to measure wind direction at wind speeds above 15 m/s aided by its polarimetric channels. In order to reduce the noise, it is necessary to decrease the spatial resolution to about 100 km and thus is mainly useful in large extra TCs. For SHOC data analysis, SMAP provides a unique opportunity to get independent surface wind speed estimates, nearly coincident with S-1A acquisitions. Hereafter, we rely on SMAP winds from RSS [17]. SMAP data have a spatial resolution of 40 km. As finally obtained, more than 8500 co-located S-1 NRCS can then be compared with SMAP wind speed estimates, ranging up to 48 m/s.

III. Data Analysis

A. NRCS

Lester, was named on August 25, with tracks and wind speed history reported in Fig. 1. On August 31, SAR images were acquired, corresponding to a reintensification phase. As obtained, both channels capture the eye location, associated with low backscatter signals, as well as strong NRCS gradient near the eyewall. The estimated eye diameter is around 20 km, and the radius of maximum backscattered intensity is about 15 km. The outer principal rain band appears as a dark curved feature, with a jagged but sharp inner edge. At the tail of the rain band, an increasing occurrence of curved features can be delineated like paw prints in the outer convective band. These features generally correspond to the leading edge of gust fronts. Circular dark bands are also observed around the eye, resulting from different effects: damping of short surface waves by heavy raindrop impacts, a decrease in the horizontal component of the surface wind at the leading edge of the band where updrafts might be at maximum, and attenuation of the signal by the intense rain in the atmosphere.

Using the method proposed in [18], NRCS inhomogeneities in SAR images can be detected. In Fig. 2 (middle), red areas have been detected, and further filtered out. NRCS variations

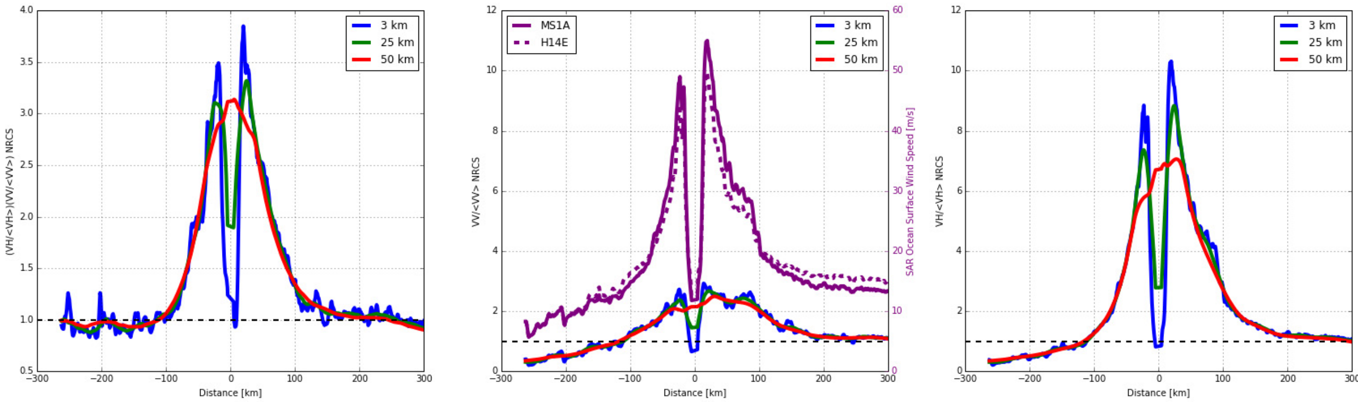

Fig. 2. Lester hurricane on August 31, 2016 at 03:16 UTC. Variation of the NRCS across the hurricane eye with respect to the background NRCS (far from the eye) for three different resolutions: 3 (blue curve), 25 (green curve), and 50 km (red curve). Pixel spacing is 1 km. (a) Ratio (VH/VV) of the variation of the NRCS. (b) Variation for VV-NRCS. Purple dotted and solid lines, respectively, stand for wind speed obtained using H14E and MS1A GMF. (c) Variation for VH-NRCS.

in both co-polarization and cross polarization can then be analyzed along transect through the hurricane eye (see the blue transect in Fig. 1). This transect is chosen to correspond to a fixed incidence angle, about 40°, minimizing NESZ fluctuation within the image subswath. A relative variation of NRCS with respect to the background signal is then defined as

$$C^{\mathrm{PP}} = \sigma_0^{\mathrm{PP}} / < \sigma_0^{\mathrm{PP}} >_{\mathrm{dist}>100\mathrm{km}}. \tag{1}$$

For both VV and CP, the background signal is defined as the averaged NRCS (in linear unit), far from the eye, i.e., a distance (D) from the eye larger than 100 km. Fig. 2(a)–(c), respectively, shows C^{VV}, C^{VH}, and the ratio between $C^{\mathrm{VH}}/C^{\mathrm{VV}}$ for three resolutions: 3 (blue), 25 (green), and 50 km (red) across hurricane Lester eye. As already reported (see [3, Fig. 10]), the NRCS contrast variations are significantly higher in VH than in VV. At 3-km resolution, C^{VH} reaches up to ten, while C^{VV} is about three. As anticipated, spatial smoothing attenuates the sensitivity difference. At 50-km smoothed resolution, maxima are integrated and now a single peak emerges around the eye. Nevertheless, the ratio between C^{VH} and C^{VV} is still significant (around factor 3 instead of 3.75 at 3 km).

As mentioned earlier, remote sensing of high wind speed is mostly controlled by the sensor capability to directly or indirectly probe the wave breaking impacts. Concerning active measurements, the differing sea state development with larger wave breaking signatures as well as foam and bubble impacts on the ocean surface dielectric and geometrical properties have been analyzed with altimeter measurements (see [19], [20]). For gale to storm conditions, [21], followed by [22] and [23], exploited the apparent altimeter signal backscatter sensitivity to propose empirical relationships with wind speeds. At larger incidence angles, scatterometer, and SAR configurations, backscatter signals are generally more strongly related to small resonant surface scatters, but are also sensitive to breaking events (see [24]). Under extreme conditions, larger wave scales are breaking and can become a very active source to generate shorter scale roughness (see [4, eq. (40)]). This can help maintain a certain polarization sensitivity between co-polarized signals ratio HH/VV but also mostly contributes to increase the cross-polarized backscatter signals. For moderate to high winds, the wind speed sensitivity of large incidence backscatter signals for both co- and cross-polarized measurements is then comparable. As obtained and illustrated in Fig. 2, both signals can indeed well trace the expected large wind gradients, i.e., the eyewall in the inner core region, with expected rapid increases of breaking occurrence and intensity. But larger breakers not only increase areas covered by very rough elements, they also generate larger and thicker foam patches (see [25]). These latter two aspects (coverage and thickness) have significant impacts on passive radiometric measurements.

TABLE II

COEFFICIENTS FOR THE CP-NRCS MS1A GMF

θ	A_1	a_1	U_{t1}	a_2	U_{t2}	a_3	U_{t3}	a_4	U_{t4}	a_5
20.00	11.5e-05	0.99	9.00	2.35	12.00	2.11	14.00	1.72	35.00	0.39
22.50	23.33e-05	0.66	8.60	2.10	14.75	2.46	15.00	1.38	42.00	1.05
25.00	7.18e-05	1.18	9.00	2.21	13.00	1.95	15.00	1.52	35.25	1.14
27.50	5.33e-05	1.30	8.50	2.06	14.00	1.87	15.00	1.51	39.00	1.08
30.00	10.0e-05	0.96	7.50	1.74	14.00	2.29	16.00	1.53	37.00	1.00
32.50	2.79e-05	1.50	10.00	2.05	15.00	2.42	18.00	1.50	34.00	0.97
35.00	2.06e-05	1.57	8.00	2.18	10.50	2.17	15.50	1.77	30.00	1.04
40.00	1.08e-05	1.80	8.50	2.38	13.50	2.08	18.00	1.59	31.00	1.32
45.00	5.79e-06	1.97	6.40	2.40	14.00	1.92	31.00	2.13	32.00	1.35

Based on Radarsat-2 data acquired in ScanSAR mode, [6] proposed two relationships to relate the CP NRCS in terms of ocean surface wind speeds: H14S and H14E geophysical model functions (GMFs). As observed in [6, Fig. 3], H14S predicts a saturation of the NRCS for ocean surface wind speed larger than 35 m/s and incidence angles lower than 45°. According to their analysis, VH-NRCSs are expected to be lower than −20 dB for extremes. Sentinel-1 data acquired during SHOC exhibit several acquisitions with NRCS larger than −20 dB. Moreover, although consistently (spatial and temporal differences) co-located with SFMR data, Radarsat-2 SAR NRCS database is considered small with possible sampling error according to the authors. In the following, we discard H14S and consider only H14E GMF that does not saturate for winds higher than 35 m/s. H14E, the second GMF, has been derived from Radarsat-2 VH-NRCS and ECMWF winds co-locations. Spatial and

This article has been accepted for inclusion in a future issue of this journal. Content is final as presented, with the exception of pagination.

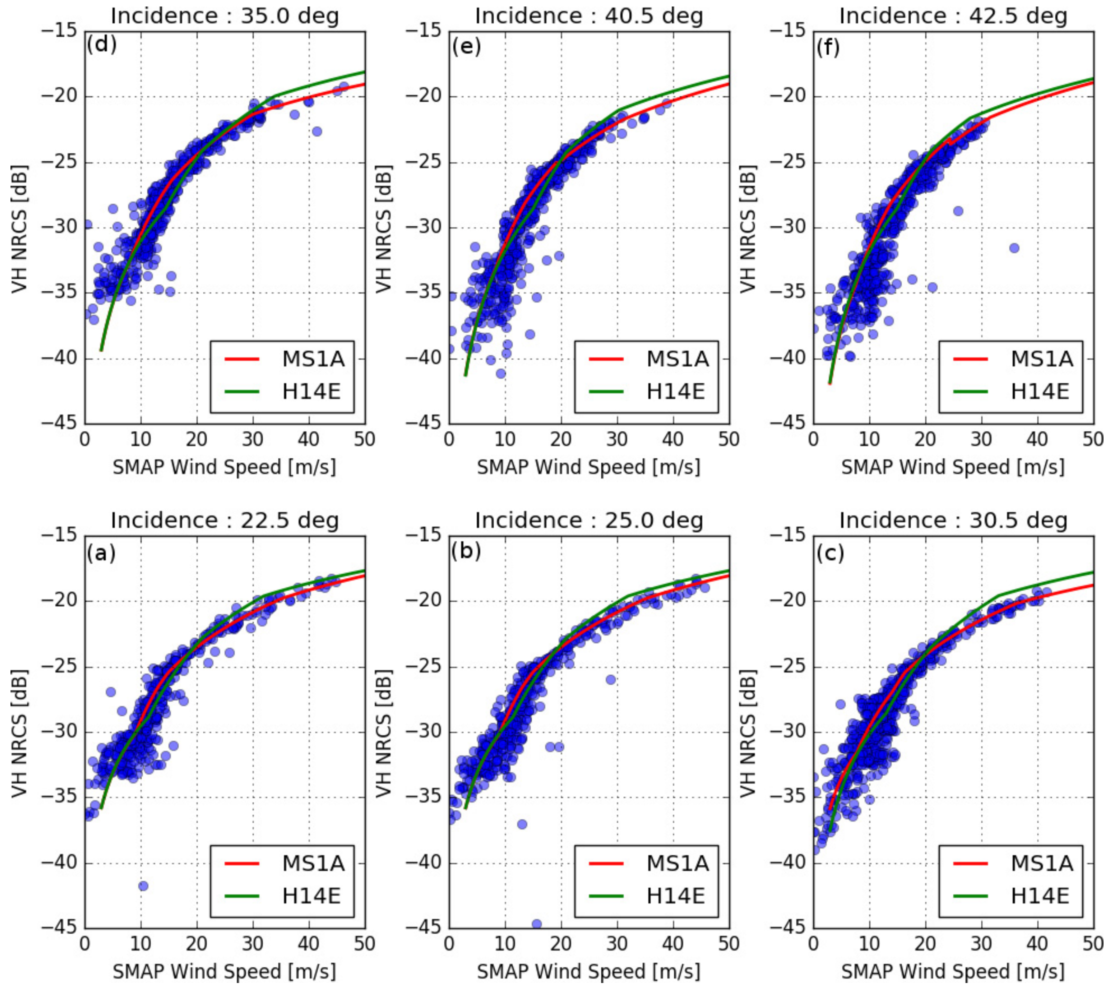

Fig. 3. 40-km VH-NRCS with respect to SMAP ocean surface wind speed for different incidence angles. (a) 22.5°. (b) 25.0°. (c) 30.5°. (d) 35.0°. (e) 40.5°. (f) 42.5°. Green and red solid lines, respectively, stand for H14E and MS1A GMF.

temporal resolutions (0.25° or about 25-km grids, 3-h time steps) of the numerical simulations are considered as coarse by [6] but allow a larger data set to work with. As observed (see [6, Fig. 3 (left)]), there is no NRCS measurement for ocean surface wind speeds larger than 35 m/s. Beyond this limit, the GMF accuracy certainly decreases. ECMWF maximum winds and maximum sustainable winds from the track (for the cases we have in SHOC) differences are found to be underestimated and wind dependent (not shown). This underestimate increases with respect to hurricane strength. This is certainly due to the difference in space and time resolution between these two sources. We expect both the duration and area of the MSW to decrease with hurricane strength. An MSW of 60 m/s during 1 min corresponds to a sustainable wind over about 3 km. These make very unlikely the possibility for the model at 0.25° to predict a maximum wind speed of 60 m/s corresponding to 1-min MSW. In addition to the issue regarding the choice of a reliable data set to be used as a reference, the number of SAR scenes acquired over hurricanes remains very low. In the contrary, the GMF used for SMAP winds has been defined to reproduce SFMR winds after corrections due to these two sensors resolution differences and benefited for a larger co-locations' dataset (see [17]). As a consequence, we propose a new GMF based on Sentinel-1A NRCS measurements and SMAP wind speeds. For that purpose, the NRCSs are computed at 40-km resolution onto the SMAP grid. The idea is to be able to be consistent with track files for maximum wind speeds derived at 3 km but also with SMAP wind fields when SAR winds are derived at 40 km. Sentinel-1 VH-NRCSs as a function of SMAP winds are presented in Fig. 3. For CP signals, the incidence angle dependency, initially found for low to moderate wind speeds (about 7 dB at 10 m/s for incidence angles ranging from 17° to 45° [10]), tends to completely vanish for SMAP estimated wind speeds larger than 30 m/s. As anticipated, especially for the lowest incidence angles and above gale wind conditions (>20 m/s), the VV NRCS is found to be much less sensitive than VH-NRCS with increasing SMAP wind speed (not shown). To note, the incidence angle dependency also strongly decreases for VV-NRCS with increasing winds. This analysis illustrates how congruous Sentinel-1 40-km VH-NRCSs become with respect to the SMAP estimated surface wind speeds. An analytical formulation is proposed to fit these measurements with respect to wind speed and incidence angle. It writes

$$\sigma_0^{\mathrm{VH}}(\theta, |\mathbf{U}_{10}|) = A_{n-1}(\theta) U_{t_{n-1}}^{a_{n-1}}(\theta) \quad (2)$$

with

$$A_n(\theta) = A_{n-1} U_{t_n}^{a_{n-1}-a_n}, \text{ if } n > 1. \quad (3)$$

In this formulation, σ_0^{VH} stands for the NRCS. σ_0^{VH} is dimensionless and expressed in linear scale. A_n and a_n are dimensionless coefficients. U_{t_n} is expressed in m/s and stands for the 10-m height ocean surface wind speed values corresponding to transitions in the NRCS regime. The values for subscript n to be used in the GMF depends on the 10-m high ocean surface wind speed $|\mathbf{U}_{10}|$ expressed in m/s. If $|\mathbf{U}_{10}| < U_{t_1}, n = 2$; if $U_{t_1} < |\mathbf{U}_{10}| < U_{t_2}, n = 3$; if $U_{t_2} < |\mathbf{U}_{10}| < U_{t_3}, n = 4$; *and* if $|\mathbf{U}_{10}| > U_{t_4}, n = 5$. Coefficients are reported in Table II.

B. SAR Winds

The present analysis of coincident co- and cross-polarized NRCS well illustrates the potential complementarity of these two channel measurements. VV-NRCS is known to be very robust for wind vector estimates from low to high wind regimes, with low signal-to-noise ratio and sensitivity to ocean wind direction. Whereas VV-NRCS sensitivity is decreasing under more extreme conditions, CP-NRCS still exhibits significant sensitivity. To date, no evidence of any wind direction dependency has been found in CP signals over TCs.

Portabella *et al.* [8] proposed a methodology combining SAR information with *a priori* information. This method is routinely applied to Sentinel-1 NRCS measurements and ocean wind vector from ECWMF (spatial resolution is 0.125° with a time step of 3 h) to produce the ESA Sentinel-1 Level-2 OCN product. It relies only on the co-polarized channel and CMOD-IFR2 GMF. Gaussian errors are considered for observations, GMF, and the model information. This leads to a minimization problem for the determination of the maximum probability to get a wind vector (speed and direction). This writes

$$J(u_{10}, v_{10}) = \left[\frac{\sigma_0^{\mathrm{PP}} - \mathrm{GMF}^{\mathrm{PP}}(\theta, \phi, |\mathbf{U}_{10}|)}{\Delta\sigma_0^{\mathrm{PP}}}\right]^2 + \left[\frac{u_{10}^{\mathrm{ECMWF}} - u}{\Delta u_{10}}\right]^2 + \left[\frac{v_{10}^{\mathrm{ECMWF}} - v}{\Delta v_{10}}\right]^2. \quad (4)$$

For the minimization, the space of solution for the radar cross-section values is computed from the GMF relationship and is directly driven by the input parameters resolution. Wind speed is defined from 0 to 80 m/s with a resolution of 0.1 m/s. Wind direction with respect to the azimuth angle is defined from 0° to 360° with a resolution of 0.5°. Then u and v components are defined such as $u = |\mathbf{U}_{10}|\cos(\theta)$ and $v = |\mathbf{U}_{10}|\sin(\theta)$. Incidence angle is defined from 17° to 45° with a resolution of 0.1°. $\Delta u_{10} = \Delta v_{10} = 2$ m/s. PP = VV, when considering only VV channel and $\Delta\sigma_0^{\mathrm{PP}} = 0.1$. These values are chosen to stick to the ocean wind algorithm as implemented in the ESA Level-2 Ocean product processor. We use CMOD5n [26] GMF to retrieve ocean surface wind from VV channel. A fourth term similar to the first one but with PP = VH can be added in (4) to consider VH channel. The choice of $\Delta\sigma_0^{\mathrm{VH}}$ is dictated by the local signal-to-noise ratio, to optimize the use of this channel to situations and locations where the information is expected to be of good quality. In particular, despite the NESZ correction, the impact of the NESZ can remain significant at subswath limits and for low values of NRCS [10]. GMF used is H14E from [6]. To note, CP signals alone can also be directly used for wind inversion with this method.

Fig. 4(a)–(c) presents the wind field retrieved at 3 km from Sentinel-1A measurements when using VV-NRCS alone combined with CMOD5n, CP-NRCS alone combined with H14E, and both VV- and CP-NRCS (combined with CMOD5n and H14E), respectively. This SAR acquisition was done on August, 27, 2016 between 20:49 and 20:55 UTC off the south east coasts of Japan over Lionrock Typhoon. Lionrock reaches its most intense stage the same day at 6 UTC, and on August, 28 between 6 and 12 UTC.

As obtained, SAR wind inversion can be significantly different depending on the polarization used for wind inversion. The poor quality of Sentinel-1 NESZ dramatically impacts the wind field retrieved from CP signals, with unrealistic jumps at each subswath limit. The noise mostly impacts areas with low signal-to-noise ratio. Near the Typhoon eye, where the strongest CP-NRCS values and gradients are measured, subswath jumps and retrieved wind speed modulation vanish. With a much higher signal-to-noise ratio, the wind derived from the co-polarized channel is not impacted. Far from the eye, where the wind is not expected to be extreme, high-resolution SAR measurement clearly reveals local gap winds. In the sea of Japan, on the north west coast of the Honshu Island, wind speed gradients of more than 10 m/s are indeed estimated to occur over few kilometers.

Near the typhoon eye, the VV estimated wind speeds are significantly lower than those obtained with VH, in line with previously reported results (see [2]). As obtained, the optimized use of co- and cross-polarized information seems to provide a realistic wind field, showing a consistent pattern of closed circulation. Over areas with relatively moderate to high wind speeds, CP is more penalized. The possible noise contamination is minimized and VV NRCS dominates. Over increasingly strong wind areas, CP NRCSs with better SNR values become more useful, and estimated wind magnitudes and gradients are likely better recovered. For this particular case, the maximum 3-km SAR wind speed estimated using VV is 33 m/s, whereas we obtain 53 m/s with VV and VH. At this time, best track indicates a maximum wind speed between 54 and 57 m/s. For the acquisition over Lester on August 31 presented in Fig. 1, 3-km SAR wind estimates indicate a maximum wind speed of 28 m/s when using VV and 54 m/s with co- and cross-polarizations' combination. Track file gives 60 m/s. These two examples, corresponding to the most intense situations we have been able to sample during SHOC, illustrate the benefit of cross-polarization channel for extreme winds.

For the acquisition over Lionrock, a co-location with SMAP with a time difference lower than 30 min exists; 40-km SMAP

This article has been accepted for inclusion in a future issue of this journal. Content is final as presented, with the exception of pagination.

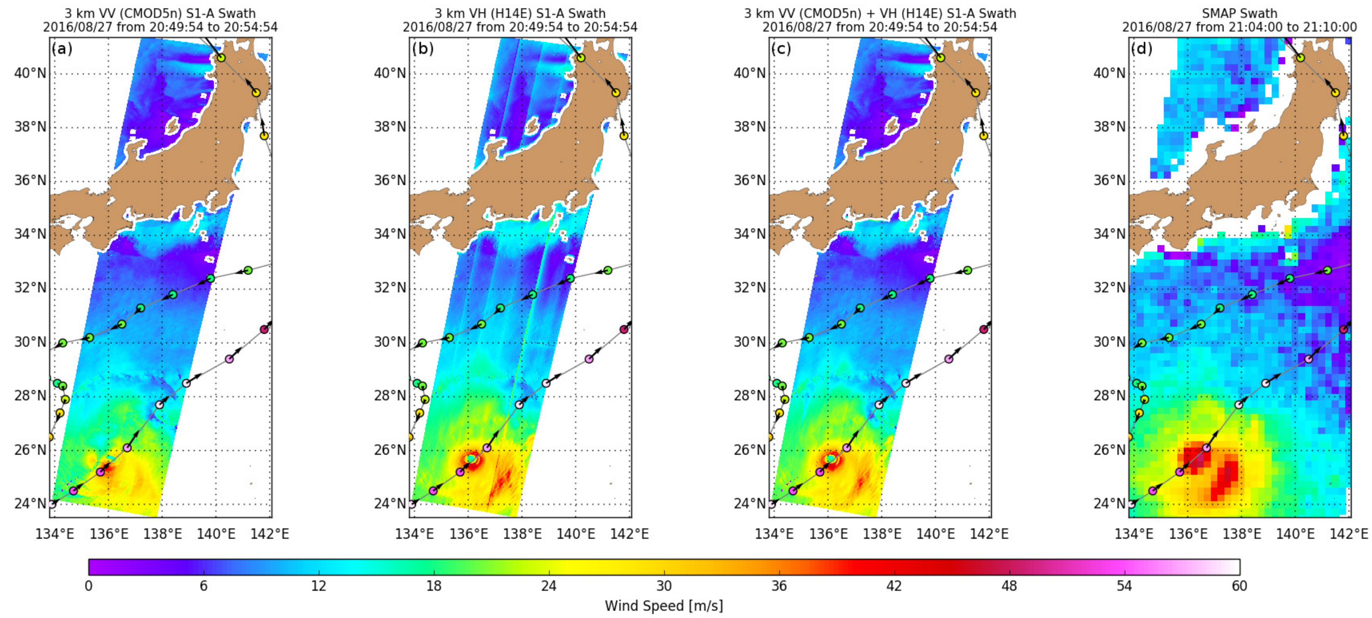

Fig. 4. Lyonrock Typhoon on August 27, 2016. 3-km resolution ocean surface wind speed measured by Sentinel-1A SAR using (a) VV polarization and CMOD5n GMF, (b) VH polarization and H14E GMF, and (c) both VV and VH polarizations with CMOD5n and H14E GMF. (d) 40-km resolution ocean surface wind speed measured by SMAP. SAR and SMAP acquisition times are, respectively, around 20:51 UTC and 21:07 UTC.

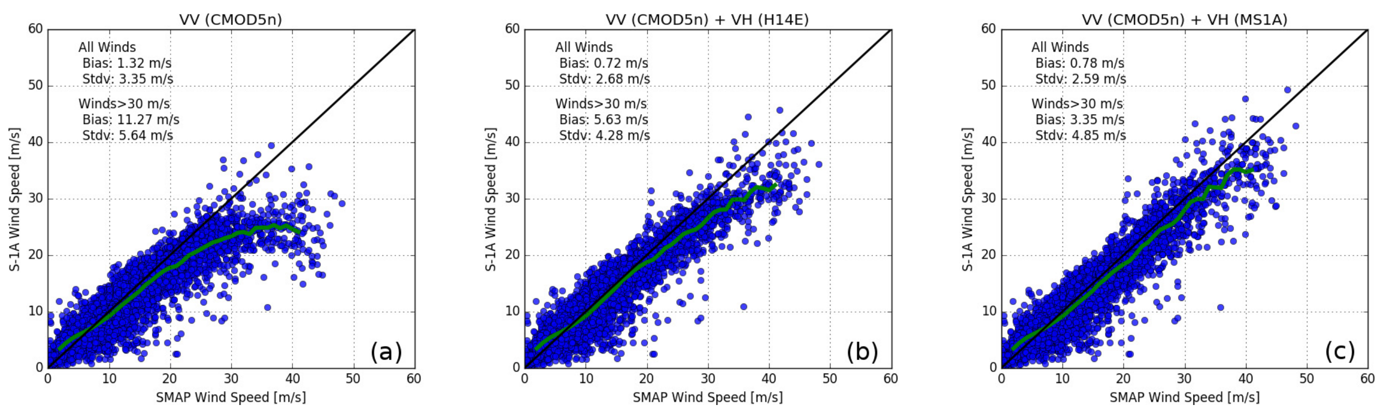

Fig. 5. 40-km SMAP wind versus 40-km SAR wind. SAR winds have been obtained using only (a) VV polarization with CMOD5n GMF, (b) VV polarization with CMOD5n GMF and VH polarization using H14E GMF, and (c) VV polarization with CMOD5n GMF and VH polarization using MS1A GMF.

wind map is shown in Fig. 4 (left) and reveals an overall good agreement with SAR wind maps. Areas with large wind speed gradients are solely detected with SAR measurements, i.e., the gap wind region and the area near the Typhoon eye. At the time of satellite acquisitions, Lionrock was at its maximum of intensity with an eye radius lower than 40 km. As observed, the eye is smeared out with SMAP measurements. The SMAP 40-km maximum wind speed is about 49 m/s.

This value cannot be directly compared with 3-km SAR winds as the resolution is different. To this aim, SAR winds are also retrieved at 40-km resolution and then compared with co-located SMAP winds. Comparison including all available cases from SHOC is shown in Fig. 5. Comparison based on SAR winds derived using only VV combined with CMOD5n is shown in Fig. 5(a). The same comparison for SAR winds relying on co- and cross-polarization channels combined with CMOD5n and H14E GMFs is shown in Fig. 5(b). Differences between both approaches show that the use of VH enables us to retrieve higher SAR wind speeds than with VV. SAR wind obtained using the two channels is more consistent with SMAP winds, in particular for the high wind speeds. When considering all the winds speeds, bias and standard deviation obtained for VV winds are, respectively, 1.3 and 3.4 m/s, whereas the use of both VV and VH gives 0.7 and 2.7 m/s. When considering only wind speeds corresponding to SMAP wind larger than 25 m/s, we obtain a bias of 8.1 $\pm$ 5.7 m/s for VV SAR wind and 4.2 $\pm$ 4.1 m/s for VV+VH SAR winds.

The same analysis has been performed to assess the impact of the new GMF in the inversion scheme. Comparisons between SMAP winds and SAR winds combining VV and VH channels with this GMF for VH are presented in Fig. 5(c). When considering all the wind speeds, bias and standard deviation are now 0.8 and 2.65 m/s. For SMAP wind

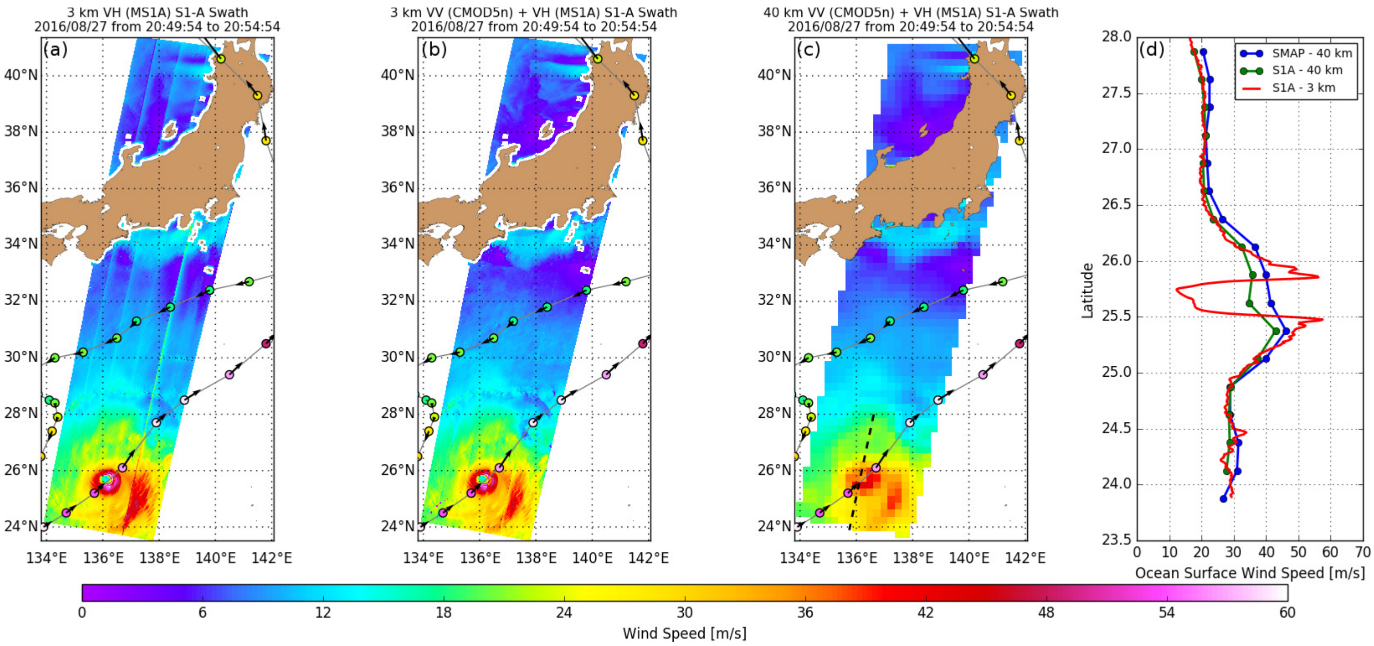

Fig. 6. Lyonrock Typhoon on August 27, 2016. 3-km resolution ocean surface wind speed measured by Sentinel-1A SAR using (a) VH polarization and MS1A GMF and (b) both VV and VH polarizations with CMOD5n and MS1A GMF. (c) 40-km resolution ocean surface wind speed measured by SAR. NRCS averaging has been done on the exact same grid as SMAP acquisition [see Fig. 4(d)].

larger than 25 m/s, we obtain a bias of 2.6 ± 4.5 m/s. Fig. 6(a) and (b) presents the results obtained with the proposed GMF for Lyonrock case at 3- and 40-km resolutions. As expected, SAR winds obtained at 40-km resolution are now more consistent with SMAP winds; 3-km resolution maximum SAR wind obtained for this case is about 64 m/s. Fig. 6(d) quantifies the wind speed variation across the typhoon eye due to the resolution differences. Along the transect, SAR winds are calculated with 3- and 40-km resolutions; 3-km SAR winds are estimated with a pixel spacing of 1 km; 40-km SAR winds are computed onto the SMAP grid. As evaluated using the 3-km resolution, from the Typhoon center to the detected maximum, wind speeds vary between 10 and 55 m/s. At 40-km resolution, SAR wind speeds vary from only 32 to 42 m/s. The relative variation of the 40-km SAR wind is in close agreement with SMAP along the whole transect. To note, for Lester, Fig. 1(e) shows the wind map obtained on August 31 with the proposed GMF; 3-km resolution maximum SAR wind is 60.5 m/s. Having a backscattered signal without any saturation and at very high resolution also offers the unique capability of retrieving the RMW. For Lyonrock, SAR gives 18 km whereas the track indicates 22 km. As observed with SMAP, in such intense phase where the radius is generally small, medium-resolution sensors are limited. For Lester, on August 31 [see Fig. 1 (right)], 3-km SAR wind estimates indicate an RMW around 15 km, while it is 28 km according to the best track.

IV. Conclusion

During summer 2016, the ESA SHOC campaign was dedicated to hurricane observations from Sentinel-1A SAR in both VV and VH polarizations in wide swath modes. About 20 images over TC eyes were acquired. Although time consuming for the ESA mission planning team, this strategy for late programing acquisitions based on hurricane track forecasts has demonstrated interesting perspectives to maximize observations of such extreme events. Indeed, hurricanes trajectories are now well forecasted in comparison with intensity [27]. Moreover, the recent launch of the Sentinel-1B and the capabilities of Radarsat-2 should enable joint analysis of the same event with respect to time.

The differing sensitivity between contemporaneous co- and cross-polarized SAR signals can be advantageously exploited to infer local information about the TC structure. To first order, SAR measurements can thus accurately document the ocean surface response in and around TC eyes. For instance, during Lester most intense phase, when the track file indicates wind speed reaching 120 knots, the sensitivity of the VH-NRCS, computed at 3-km resolution, is more than 3.5 times larger than in VV. This very large sensitivity can provide accurate estimates of the eye diameter and the RMW speed. The use of the background wind speed (lower than 25 m/s) as obtained in co-polarization has already been coupled with Holland parametric wind model to retrieve maximum wind speed in co-polarization [28]. The higher sensitivity of the cross polarization should allow us to refine such an approach and help reviewing parametric model performances.

A new method is developed to merge information from both VV and VH channels. It improves the accuracy of the ocean surface wind speed for winds larger than 25–30 m/s and shows the potential of using CP channel with Sentinel-1 C-SAR sensor. The unique opportunity to co-locate Sentinel-1A SAR acquisitions with SMAP radiometer is used to refine the relationship between VH NRCS at C-band and ocean surface wind from SMAP. The use of this new GMF ensures a very good consistency between SAR and

SMAP winds. This paper also shows that Sentinel-1A data are more consistent with H14E than H14S GMF proposed in [6]. To note, for wind speed retrieval algorithms, the availability of reliable reference data representative of few kilometers wind measurement remains obviously a challenge. From the 20 hits obtained during SHOC, only one acquisition could be co-located with SFMR. Yet for this case, the wind was not exceeding 35 m/s in agreement with SAR winds' estimate.

In the context of the forthcoming MeTop-SG scatterometer (SCA), the ability of Sentinel-1 SARs to get NRCS measurements at high resolution in both co-polarization and cross polarization will certainly help new algorithms' developments. The estimate of NRCS at scatterometer resolution should enable us to quantitatively assess the resolution impact on cross-polarization channel sensitivity inside the 34-knot wind radii where MeTop-SG SCA is expected to improve the wind speed accuracy.

Finally, there are certainly studies to be undertaken to co-analyze brightness temperatures from radiometers and NRCS from active radar. This could help deciphering between the respective contributions of foam patches and large breakers to the NRCS sensitivity for extremes.

Acknowledgment

The authors would like to thank P. Potin, B. Rosich, N. Miranda, and Y.-L. Desnos at ESA for their support to set up the SHOC campaign. They would also like to thank J. Roeder and A. Duchini from the Sentinel-1 mission planning team for their efforts and reactivity during the campaign. This has been the key for late programing acquisitions. This paper relies on Copernicus Sentinel-1 SAR data. SMAP winds are from Remote Sensing Systems (available online at www.remss.com/missions/smap).

References

[1] K. B. Katsaros, P. W. Vachon, P. G. Black, P. P. Dodge, and E. W. Uhlhorn, "Wind fields from SAR: Could they improve our understanding of storm dynamics?" *Johns Hopkins APL Tech. Dig.*, vol. 21. 2000, pp. 86–93.

[2] B. Zhang and W. Perrie, "Cross-polarized synthetic aperture radar: A new potential measurement technique for hurricanes," *Bull. Amer. Meteorol. Soc.*, vol. 93, no. 4, pp. 531–541, 2012.

[3] J. W. Sapp, S. O. Alsweiss, Z. Jelenak, P. S. Chang, S. J. Frasier, and J. Carswell, "Airborne co-polarization and cross-polarization observations of the ocean-surface NRCS at C-band," *IEEE Trans. Geosci. Remote Sens.*, vol. 54, no. 10, pp. 5975–5992, Oct. 2016.

[4] V. Kudryavtsev, I. Kozlov, B. Chapron, and J. A. Johannessen, "Quad-polarization SAR features of ocean currents," *J. Geophys. Res., Oceans*, vol. 119, no. 9, pp. 6046–6065, 2014.

[5] P. A. Hwang, B. Zhang, and W. Perrie, "Depolarized radar return for breaking wave measurement and hurricane wind retrieval," *Geophys. Res. Lett.*, vol. 37, no. 1, p. L01604, 2010.

[6] P. A. Hwang *et al.*, "Cross-polarization geophysical model function for C-band radar backscattering from the ocean surface and wind speed retrieval," *J. Geophys. Res., Oceans*, vol. 120, no. 2, pp. 893–909, 2015. [Online]. Available: http://dx.doi.org/10.1002/2014JC010439

[7] B. Zhang *et al.*, "Ocean vector winds retrieval from C-band fully polarimetric SAR measurements," *IEEE Trans. Geosci. Remote Sens.*, vol. 50, no. 11, pp. 4252–4261, Nov. 2012.

[8] M. Portabella, A. Stoffelen, and J. A. Johannessen, "Toward an optimal inversion method for synthetic aperture radar wind retrieval," *J. Geophys. Res.*, vol. 107, no. C8, pp. 1-1–1-13, 2002.

[9] A. A. Mouche *et al.*, "On the use of Doppler shift for sea surface wind retrieval from SAR," *IEEE Trans. Geosci. Remote Sens.*, vol. 50, no. 7, pp. 2901–2909, Jul. 2012.

[10] A. Mouche and B. Chapron, "Global C-band Envisat, RADARSAT-2 and Sentinel-1 SAR measurements in copolarization and cross-polarization," *J. Geophys. Res., Oceans*, vol. 120, no. 11, pp. 7195–7207, 2015.

[11] E. V. Zabolotskikh, L. M. Mitnik, and B. Chapron, "New approach for severe marine weather study using satellite passive microwave sensing," *Geophys. Res. Lett.*, vol. 40, no. 13, pp. 3347–3350, 2013.

[12] N. Reul, J. Tenerelli, B. Chapron, D. Vandemark, Y. Quilfen, and Y. Kerr, "SMOS satellite L-band radiometer: A new capability for ocean surface remote sensing in hurricanes," *J. Geophys. Res., Oceans*, vol. 117, no. C2, pp. 1–24, 2012.

[13] S. H. Yueh *et al.*, "SMAP L-band passive microwave observations of ocean surface wind during severe storms," *IEEE Trans. Geosci. Remote Sens.*, vol. 54, no. 12, pp. 7339–7350, Dec. 2016.

[14] S. Banal, S. Iris, and R. Saint-Jean, "Canadian Space Agency's Hurricane Watch Program: Archive contents, data access and improved planning strategies," in *Proc. IEEE Int. Geosci. Remote Sens. Symp.*, Jul. 2007, pp. 3494–3497.

[15] C. Velden *et al.*, "The Dvorak tropical cyclone intensity estimation technique: A satellite-based method that has endured for over 30 years," *Bull. Amer. Meteorol. Soc.*, vol. 87, no. 9, pp. 1195–1210, 2006.

[16] J. A. Knaff, C. J. Slocum, K. D. Musgrave, C. R. Sampson, and B. R. Strahl, "Using routinely available information to estimate tropical cyclone wind structure," *Monthly Weather Rev.*, vol. 144, no. 4, pp. 1233–1247, 2016.

[17] T. Meissner, L. Ricciardulli, and F. J. Wentz, "Capability of the SMAP mission to measure ocean surface winds in storms," *Bull. Amer. Meteor. Soc.*, [Online]. Available: https://doi.org/10.1175/BAMS-D-16-0052.1

[18] W. Koch, "Directional analysis of SAR images aiming at wind direction," *IEEE Trans. Geosci. Remote Sens.*, vol. 42, no. 4, pp. 702–710, Apr. 2004.

[19] Q. A. Zheng, V. Klemas, G. S. Hayne, and N. E. Huang, "The effect of oceanic whitecaps and foams on pulse-limited radar altimeters," *J. Geophys. Res., Oceans*, vol. 88, no. C4, pp. 2571–2578, 1983.

[20] Y. Quilfen, J. Tournadre, and B. Chapron, "Altimeter dual-frequency observations of surface winds, waves, and rain rate in tropical cyclone Isabel," *J. Geophys. Res., Oceans*, vol. 111, no. C1, pp. 1–13, 2006.

[21] I. R. Young, "An estimate of the Geosat altimeter wind speed algorithm at high wind speeds," *J. Geophys. Res., Oceans*, vol. 98, no. C11, pp. 20275–20285, 1993.

[22] Y. Quilfen, B. Chapron, T. Elfouhaily, K. Katsaros, and J. Tournadre, "Observation of tropical cyclones by high-resolution scatterometry," *J. Geophys. Res., Oceans*, vol. 103, no. C4, pp. 7767–7786, 1998.

[23] Y. Quilfen, D. Vandemark, B. Chapron, H. Feng, and J. Sienkiewicz, "Estimating gale to hurricane force winds using the satellite altimeter," *J. Atmos. Ocean. Technol.*, vol. 28, no. 4, pp. 453–458, 2011.

[24] O. M. Phillips, "Radar returns from the sea surface—Bragg scattering and breaking waves," *J. Phys. Oceanogr.*, vol. 18, no. 8, pp. 1065–1074, 1988.

[25] N. Reul and B. Chapron, "A model of sea-foam thickness distribution for passive microwave remote sensing applications," *J. Geophys. Res., Oceans*, vol. 108, no. C10, 2003.

[26] H. Hersbach, "Comparison of C-band scatterometer CMOD5.N equivalent neutral winds with ECMWF," *J. Atmos. Ocean. Technol.*, vol. 27, no. 4, pp. 721–736, 2010.

[27] M. DeMaria *et al.*, "Improvements to the operational tropical cyclone wind speed probability model," *Weather Forecasting*, vol. 28, no. 3, pp. 586–602, 2013.

[28] A. Reppucci, S. Lehner, J. Schulz-Stellenfleth, and S. Brusch, "Tropical cyclone intensity estimated from wide-swath SAR images," *IEEE Trans. Geosci. Remote Sens.*, vol. 48, no. 4, pp. 1639–1649, Apr. 2010.

Alexis A. Mouche received the Ph.D. degree in ocean remote sensing from the Université de Versailles Saint-Quentin, Versailles, France, in 2005.

He currently a Senior Research Scientist with the Laboratoire d'Océanographie Physique et Spatiale, Institut Francais de Recherche pour l'Exploitation de la Mer, Plouzane, France, since 2014. His research interests include the interaction of electromagnetic and oceanic waves for ocean remote sensing applications.

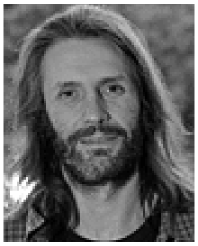

Bertrand Chapron received the Ph.D. degree in fluid mechanics from Aix–Marseille University, Marseille, France, in 1988.

He is currently a Senior Research Scientist with the Laboratoire d'Océanographie Physique Spatiale, Institut Francais de Recherche pour lâ'Exploitation de la Mer, Plouzane, France. He has been the Co-Investigator or Principal Investigator in several ESA (ENVISAT RA2, ASAR, and SMOS), NASA, and CNES (TOPEX and JASON) projects. He contributed to the development of several algorithms for geophysical parameter retrieval from altimeters, radiometers, or SAR. He is co-responsible for the ENVISAT ASAR-Wave Mode algorithms and scientific preparation for the ENVISAT and S1 wind, wave, and current. Recently, he collaborated in studies that demonstrated the high potential of radiometers for wind retrieval in extreme conditions and the possibility of doing directional ocean waves spectrum from Sentinel-2. He has authored over 80 publications in refereed journals in applied mathematics, physical oceanography (upper ocean dynamics), and electromagnetic wave theory and its application to ocean surface remote sensing.

Biao Zhang (SM'16) received the B.S. degree in surveying and mapping engineering from the China University of Petroleum, Dongying, China, in 2003, and the Ph.D. degree in physical oceanography from the Institute of Oceanology, Chinese Academy of Sciences, Qingdao, China, in 2008.

From 2008 to 2011, he was a Post-Doctoral Fellow with the Canadian Government Laboratory, Bedford Institute of Oceanography in Dartmouth, Dartmouth, NS, Canada. In 2011, he joined the School of Marine Sciences, Nanjing University of Information Science and Technology, Nanjing, China, as a Professor. In 2015, he was a Visiting Scientist with the Department of Mechanical Engineering, University of Maryland, College Park, MD, USA. His research interests include ocean surface waves and wind fields remote sensing by along-track interferometric, multipolarization and compact polarimetric synthetic aperture radar (SAR), marine weather events such as typhoons or hurricanes monitoring with active SAR and passive radiometer observations, mesoscale eddy and cellular convection studies, spaceborne multisensor study of sea surface thermal fronts, and air-sea interaction investigation using remote sensing and numerical models.

Dr. Zhang was a recipient of the Visiting Fellow Scholarship of the Natural Sciences and Engineering Research Council of Canada. He was also a recipient of the first prize of Ocean Science and Technology from the State Oceanic Administration of China, the second prize of natural science from the Ministry of Education of China in 2014, and the Outstanding Young Scientist Award by the National Science Foundation of China in 2016.

Romain Husson received the M.Sc. Degree from the Supaero Engineering School, Toulouse, France, and the Ph.D. degree in physical oceanography from Collecte Localisation Satellites-Division des Applications Radar, Brest, France, where he was involved in developing methods to estimate synthetic swell field from SAR wave mode observations.

He was an Intern with NASA JPL, Pasadena, CA, USA, and a Young Graduate Trainee with ESRIN, Frascati, Italy, where he was involved in synthetic aperture radar wind wave current activities. Since 2013, he has been involved in several applicative and research and development projects such as wind/wave products for marine renewable energy and contributed in several ESA and European projects such as Cal/Val activities for ENVISAT and the Sentinel-1 Mission Performance Center as a Level-2 Expert. He is also involved in S1 ocean study as a Project Manager and on the technical aspects for wind, wave, and synergetic retrieval.